Materials Advances

ROYAL SOCIETY OF CHEMISTRY

PAPER

View Article Online
View Journal | View Issue

Cite this: *Mater. Adv.*, 2024, 5, 665

Thermo-responsive injectable hydrogels from linear and star-shaped block copolymers composed of amino acid-derived vinyl polymer and poly(ethylene glycol) for biomedical applications†

Mitsuki Nakamura, Shin-nosuke Nishimura, * Nobuyuki Higashi and Tomoyuki Koga *

Injectable hydrogels possess great potential in industrial, biomedical, and cosmetic applications. This study presents the synthesis and characterization of novel thermo-responsive injectable hydrogels derived from amino acid-derived vinyl polymer/polyethylene glycol (PEG) hybrid block copolymers. Two types of block copolymers, linear (**1*n***, *n* = 101, 250, 321: chain length of amino acid-based polymer block) and star-shaped (tetra-branched **2*n***, *n* = 28, 66, 118), were successfully prepared *via* atom transfer radical polymerization of *N*-acryloyl-L-alanine methyl ester (NAAMe) using PEG macroinitiators, and their gelation behaviors were comprehensively explored. In a dilute aqueous solution (1 wt%), both linear and star polymers exhibited lower critical solution temperature behavior, with a transition temperature (T_t) of 20 °C. At higher polymer concentrations, hydrogels are formed for all polymers at temperatures above T_t, with star-shaped copolymers exhibiting significantly better gelation ability (minimum gelation concentration: 6 wt% ($\mathbf{2}_{\mathbf{118}}$) and 17 wt% ($\mathbf{1}_{\mathbf{321}}$)). These block copolymers respond rapidly to temperature changes, facilitating instant gelation at body temperature through self-assembly, thus making them sophisticated injectable hydrogels. Structural factors, such as PNAAMe length and polymer shape, influence their self-assembled structure, including network density, enabling tunable mechanical properties of the gels. Furthermore, these block copolymers demonstrated good cytocompatibility and negligible macrophage activation. Thus, the PNAAMe/PEG block copolymers serve as efficient injectable three-dimensional-scaffolds for tissue engineering and controlled release.

Received 2nd November 2023,
Accepted 2nd December 2023

DOI: 10.1039/d3ma00954h

rsc.li/materials-advances

Introduction

Hydrogels are widely used in the food, engineering, biomedical, and cosmetic fields due to their water-swollen three-dimensional (3D)-network structures, which offer structural flexibility similar to that of the natural extracellular matrix (ECM) of living tissues, encapsulation ability for various substances, and biocompatibility.[1,2] In recent years, there has been a surge in research focused on developing smart hydrogels equipped with various functionalities, such as stimuli-responsiveness,[3,4] high mechanical strength,[5–7] self-healing,[8–11] shape fix/memory,[12–14] and injectability.[15–28] These smart gels are used in soft actuators, controlled-release matrices, and cell scaffolds in regenerative medicine.

Among these, injectable hydrogels, which flow like a sol (or solution) when extruded from a syringe and gelled instantaneously at the injection site, are one of the most important smart gels for biomedical applications.[15–17] Since these gels can be easily implanted in the body *via* injection, minimally invasive treatments can be performed without incisional surgery by encapsulating the appropriate drugs or cells in the gel. In addition, the hydrogel form is useful for protecting cells from membrane damage, which is often caused by mechanical forces during the injection process.[18,19] Several strategies have been employed to construct injectable gels, such as *in situ* gelling system,[20,21] shear-thinning mechanisms,[22–25] and physical cross-linking in response to physiological environments such as temperature, pH, and ion strength.[26–28] In particular, the body temperature-responsive type of injectable hydrogel is of practical significance because the temperature in a living

Department of Molecular Chemistry & Biochemistry, Faculty of Science & Engineering, Doshisha University, Kyotanabe, Kyoto, 610-0321, Japan. E-mail: tkoga@mail.doshisha.ac.jp, shnishim@mail.doshisha.ac.jp

† Electronic supplementary information (ESI) available: Structural characterization for macroinitiators and polymers; gel behaviors and biocompatibility tests of the polymers (supplemental figures). See DOI: https://doi.org/10.1039/d3ma00954h

body is relatively constant at 35–39 °C regardless of the mammal species and the specific part of the body.

Thermo-responsive polymers are fascinating building units for fabricating injectable gel systems because such polymers can switch their hydrophobic/hydrophilic characteristics or conformations solely through temperature manipulation. This characteristic is convenient for designing dynamic and reversible cross-linkages *via* noncovalent interactions. Both natural and synthetic polymers can be employed as thermo-sensitive injectable gels. For example, natural polymer-based hydrogels made from polysaccharides (chitosan, hyaluronic acid, and cellulose)[29,30] and proteins (for example, gelatin),[31] exhibit a sol–gel transition at specific temperatures. Although these natural hydrogels inherently possess excellent biocompatibility, there are still some issues, such as the difficulty in tuning their chemical structure and thermo-responsiveness. Thermo-sensitive injectable gel systems have also been developed from synthetic polymers with a lower critical solution temperature (LCST), such as poly(*N*-isopropyl acrylamide) (PNIPAM)[32,33] and poly(ethylene glycol) (PEG),[34,35] due to their quick response to dynamic temperature environments. The constituent synthetic polymers of injectable gels must be biocompatible and non-toxic for biomedical applications. PNIPAM has widely been used as the representative LCST-type polymer, since the LCST is fairly close to body temperature (32 °C) and is biocompatible. However, PNIPAM often causes undesirable biological responses, such as blood-clot formation,[36,37] especially in blood-contacting applications. Therefore, exploring new synthetic polymer systems that can act as thermo-triggered injectable hydrogels with good biocompatibility is an important challenge in developing innovative 3D-matrices for spatially controlled drug/cell delivery and tissue engineering.

Herein, we report the synthesis of linear and star-shaped block copolymers composed of LCST-type amino acid-derived vinyl polymers, poly(*N*-acryloyl alanine methyl ester) (PNAAMe), and biocompatible PEG as novel 3D-matrices with fast thermo-responsiveness and injectability (Fig. 1). Amino acid-derived vinyl polymers are promising candidates for a new class of thermo-sensitive materials.[38–47] Their thermo-responsiveness can be tuned by varying the types of amino acids (20 types) and terminal structures, and they are easy to synthesize and biocompatible.[41,42,45–47] This enables the precise design of diverse vinyl polymers with structural and functional diversity.

The thermo-responsive and self-assembling properties of the linear and star-shaped PNAAMe/PEG block copolymers, including the mechanical and injectable performances of the resultant hydrogels, were comprehensively investigated, especially with respect to the impact of the chain length of the PNAAMe blocks and the polymer shape. To demonstrate the potential of these hydrogels as injectable and biocompatible 3D matrices, their capabilities as artificial ECMs and controlled-release materials for model drugs were assessed. We believe that this study provides a useful platform for fabricating thermo-induced injectable scaffolds with versatile potential applications in the biomedical, nanotechnological, and cosmetic fields.

Experimental

Materials

L-Alanine methyl ester hydrochloride was acquired from Watanabe Chemical Industries, Ltd (Japan). *N*,*N*-Dimethlylformamide (DMF), chloroform, dichloromethane (DCM), triethylamine (TEA), tetrahydrofuran (THF), ethyl acetate, diethyl ether, hexane, dimethyl sulfoxide (DMSO), acryloyl chloride, anhydrous magnesium sulfate ($MgSO_4$), sodium sulfate (Na_2SO_4), methanol (MeOH), and ethanol (EtOH) were obtained from Nacalai Tesque, Inc. (Japan). CuBr(I), sodium chloride, and bovine serum albumin (BSA) were purchased

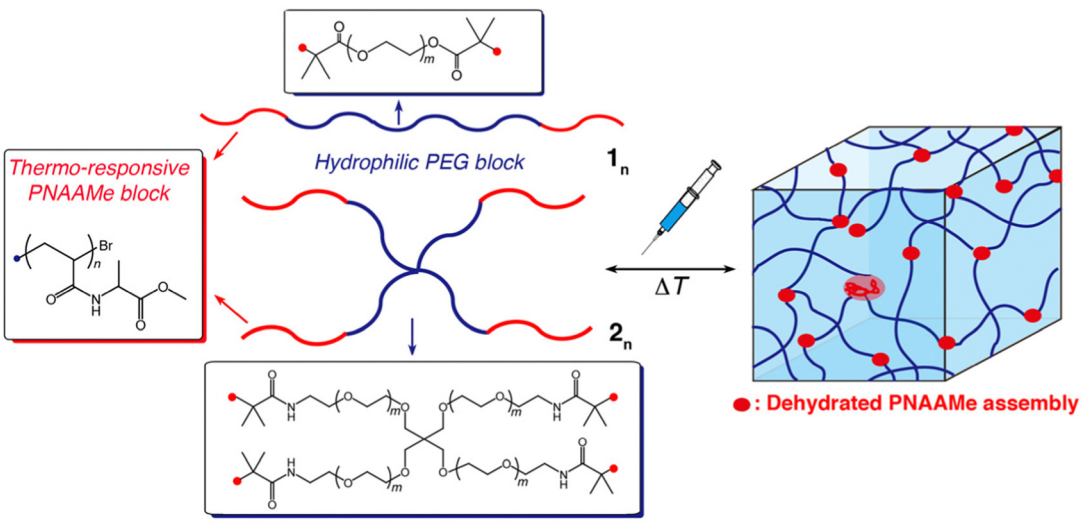

Fig. 1 Schematic illustration of the thermo-responsive injectable hydrogel formed *via* self-assembly of amino acid-derived vinyl polymer/PEG block copolymers. Chemical structures of PNAAMe/PEG block copolymers with linear (**1**$_n$) and star-shapes (**2**$_n$) used in this study.

from FUJIFILM Wako Pure Chemical Co. (Japan). 2-Bromoisobutyryl bromide (BiBB), fluorescein 5-isothiocyanate isomer I (FITC), and tris[2-(dimethylamino)ethyl]amine (Me_6TREN) were purchased from Tokyo Chemical Industry Co., Ltd (Japan). Poly(ethylene glycol) (PEG, MW = 10 000) was sourced from Sigma-Aldrich, Co. LLC (USA). Amine-terminated 4-arm PEG (4-arm PEG-NH_2, MW = 10 000) was purchased from the Biopharma PEG Scientific Inc. (USA). Doxorubicin hydrochloride (Dox) was procured from Combi-Blocks Inc. (USA). All reagents were used as received.

Synthesis of *N*-acryloyl-alanine methyl ester (NAAMe)

N-Acryloyl-alanine methyl ester was synthesized by the condensation reaction of L-alanine methyl ester hydrochloride with acryloyl chloride, as described in our previous study.[45]

Synthesis of PEG macroinitiators (linear-type and 4-arm type)

The bromo-terminated PEG (linear type) used as the macroinitiator was synthesized as follows: PEG 9.30 g (0.93 mmol) and TEA 1.30 mL (9.3 mmol) were dissolved in DCM (300 mL). BiBB 1.15 mL (9.3 mmol) in DCM (20 mL) was then added dropwise to the PEG solution. The reaction mixture was stirred overnight at ambient temperature. The solution was washed repeatedly with 1.5 M $MgSO_4$ aq. (100 mL × 4). The organic phase was collected and dried over anhydrous Na_2SO_4. After the solution was concentrated *in vacuo*, the obtained polymer was purified by reprecipitation using diethyl ether and identified by FTIR, ^{1}H- and ^{13}C-NMR spectroscopies (Fig. S1, ESI†).

The bromo-terminated 4-arm PEG (4-arm PEG-Br_4) was synthesized in the same manner using a 4-arm PEG-NH_2 1.05 g (0.11 mmol) as the starting compound. The chemical structure was identified using FTIR, ^{1}H- and ^{13}C-NMR spectroscopies (Fig. S2, ESI†).

PEG-Br_2

Yield: 7.05 g (75%). ^{1}H-NMR (500 MHz, chloroform-*d*, TMS): δ/ppm = 1.9–2.0 ppm (–CH_3: methyl of BiBB), 3.3–3.9 ppm (–CH_2CH_2O–: main chain of PEG), 4.2–4.3 ppm (–CH_2OCO–: main chain of PEG). ^{13}C-NMR (chloroform-*d*, TMS): δ/ppm = 30 ppm (–*C*H_3: methyl of BiBB), 56 ppm (*C*$(CH_3)_2$–Br: BiBB), 65 ppm (–CH$_2$*C*H$_2$–OCO–: main chain of PEG), 68 ppm (–*C*H$_2$CH$_2$–OCO–: main chain of PEG), 71 ppm (–*C*H$_2$*C*H$_2$O–: main chain of PEG), 173 ppm (–O*C*OCH$_2$: BiBB). FT-IR spectrum (KBr): 1740 cm^{-1} (C=O: ester), 1466 cm^{-1} (C–H: main chain of PEG), 1110 cm^{-1} (C–O: main chain of PEG).

4-arm PEG-Br_4

Yield: 0.91 g (86%). ^{1}H-NMR (500 MHz, chloroform-*d*, TMS): δ/ppm = 1.8–2.0 ppm (–CH_3: methyl of BiBB), 3.3–3.9 ppm (–CH_2CH_2O–: main chain of PEG), 7.1–7.2 ppm (–CON*H*CH$_2$–: amide). ^{13}C-NMR (chloroform-*d*, TMS): δ/ppm = 32 ppm (–*C*H_3: methyl of BiBB), 39 ppm (–CH$_2$*C*H$_2$–NHCO–: methyl of BiBB), 62 ppm (*C*$(CH_3)_2$–Br: BiBB), 68 ppm (–*C*H$_2$CH$_2$–NHCO–: main chain of PEG), 70 ppm (–*C*H$_2$*C*H$_2$O–: main chain of PEG), 172 ppm (–O*C*O–: BiBB). FT-IR spectrum (KBr): 1665 cm^{-1} (amide I), 1520 cm^{-1} (amide II), 1466 cm^{-1} (C–H, main chain of PEG), 1110 cm^{-1} (C–O: main chain of PEG).

Synthesis of amino acid-derived vinyl polymer/PEG block copolymers (linear and star-type)

A general method for the ATRP synthesis of the PNAAMe/PEG block copolymers is as follows: The synthesis of a linear PNAAMe (n = 101)/PEG hybrid is shown below as an example. PEG-Br_2 macroinitiator (0.3 g, 30 μmol), NAAMe (0.94 g, 6 mmol), CuBr(I) (25.8 mg, 180 μmol), and Me_6TREN (72 μL, 270 μmol) were dissolved in methanol (monomer concentration: 3 M) and charged in a glass tube. The glass tube was deoxygenated by repeating freeze–pump–N_2 filling–thaw cycle. The polymerization was carried out at 60 °C for 22 h. The polymer was isolated *via* reprecipitation using diethyl ether. The objective polymer was finally purified *via* dialysis using a Spectra/Por®7 Dialysis Membrane with an MWCO:8 kDa in distilled water and lyophilized. The resulting copolymer was characterized by ^{1}H-NMR spectroscopy (Fig. S3 and S4, ESI†) (the number average degree of polymerization (DP) of PNAAMe block was n = 101, which was calculated based on the area ratio of the signals of CH_3 and CH in Ala unit to that of CH_2 in the PEG block) and size exclusion chromatography (SEC) (eluent: DMF, PMMA standard; M_n = 42 900 and $Đ(M_w/M_n)$ = 1.14) (Fig. S5, ESI†). Other block copolymers with different DP (n) were synthesized in the same manner by changing the monomer conversion and feed ratio ([M]/[I]).

Star-shaped PNAAMe/PEG block copolymers were synthesized in the same manner as described above using 4-arm PEG-Br_4 as a macroinitiator. The results of the block copolymer synthesis are summarized in Table 1.

Measurements

^{1}H- and ^{13}C-NMR analyses were conducted using a JNM-ECA500 (JEOL Resonance Co., Ltd, Japan) spectrometer (500 MHz). The transmission FTIR spectra were measured using the KBr method with an FTIR-4600 spectrometer (JASCO Ltd, Japan). The number-average molecular weight (M_n) and the polydispersity index ($Đ = M_w/M_n$) of synthesized polymers were evaluated by SEC using a JASCO LC-net II/AD (JASCO Ltd, Japan) equipped with a refractive index (RI) detector. The measurements were conducted in DMF (10 mM LiBr) at 40 °C (flow rate of 0.6 mL min^{-1}, column: TSK-gel α-4000 (Tosoh Co., Japan)).

Table 1 Summary of PNAAMe/PEG block copolymers synthesized in this study

Polymer	Shape	$M_{n,SEC}$	$Đ$	n^a	$F_{PNAAMe}{}^b$ (wt%)
$\mathbf{1}_{101}$	Linear	42 900	1.14	101	76.0
$\mathbf{1}_{250}$	Linear	77 400	1.29	250	88.7
$\mathbf{1}_{321}$	Linear	126 000	1.23	321	91.0
$\mathbf{2}_{28}$	Star	45 700	1.13	28	63.7
$\mathbf{2}_{66}$	Star	65 500	1.14	66	80.6
$\mathbf{2}_{118}$	Star	83 800	1.17	118	88.1

[a] The number-average degree of polymerization (n) of PNAAMe per block calculated from ^{1}H-NMR analysis. [b] The weight fraction of the PNAAMe units in the polymer was calculated using the following equation: F_{PNAAMe} = MW of NAAMe × n × block number (*i.e.* 2 (linear) or 4 (star))/(MW of NAAMe × n × block number + MW of the PEG block).

Low-dispersity poly(methyl methacrylate)s (GL Sciences Inc., *M*w = 2810, 5000, 10 290, 27 600, 60 150, 138 600, and 298 900) were used as calibration standards. The transmittance of aqueous solutions of the polymers (1 wt%) was monitored at 600 nm using a V-650 spectrophotometer (JASCO Ltd, Japan) equipped with a water-cooled Peltier cell holder ETCS-761 (JASCO Ltd, Japan). The transmittance of each polymer solution was measured continuously at a constant heating rate (1 °C min^{-1}) in a quartz cell with a 1 cm path length. The rheological analyses of the hydrogels were performed using a Discover HR-1 instrument (TA Instruments Inc., USA) equipped with a Peltier device for temperature control. Measurements were performed at various temperatures using parallel plates (diameter: 40 mm). The gap between the plates was adjusted to approximately 400 μm to ensure the complete filling of the geometry. During all measurements, a solvent trap was used to minimize evaporation. The temperature-dependences of storage (G') and loss (G'') moduli were measured at 1% strain and 6.3 rad s^{-1} at a constant heating rate of 1 °C min^{-1}.

Cytocompatibility tests for the block copolymers

Mouse macrophage-like cells, RAW264.7 cells (ECACC cell bank, UK), were used for cytocompatibility test for the PNAAMe/PEG block copolymers. The cells were cultured to 80% confluence in Dulbecco's modified Eagle's medium (DMEM) (FUJIFILM Wako Pure Chemical Co., Japan) supplemented with 10% (v/v) fetal bovine serum (FBS; Sigma-Aldrich Co. LLC, USA) and 1% penicillin/streptomycin (FUJIFILM Wako Pure Chemical Co., Japan) at 37 °C under 5% CO_2.

Cytotoxicity tests by WST-8 assay. The cells were seeded in a 96-well plate (Thermo Fisher Scientific Inc., USA) at a density of 1.6×10^4 cells per mL (200 μL) per well and cultured for 24 h. The medium was then removed, and fresh medium containing the block copolymers (0.01–10 mg mL^{-1}) was added to the wells and incubated for 24 h. Commercially available PEG (MW 10 000) was used for comparison. The medium was subsequently discarded, and the cells were washed three times with fresh medium. Then, 190 μL of fresh medium and 10 μL of CCK-8 solution (Dojindo Laboratories Co., Ltd, Japan) was added to each well. The cells were incubated at 37 °C for 1 h and their absorbance was measured at 450 nm using a microplate reader (Multiskan FC, Thermo Fisher Scientific Inc., USA). The cell viability (%) was estimated relative to cells cultured in the absence of polymers (100% viability) (N = 3).

Nitric oxide (NO) assay. The cells in DMEM containing 10% FBS, 1% penicillin/streptomycin, and the block copolymers (0.01–10 mg mL^{-1}) were seeded on a 96-well plate at a density of 1.6×10^5 cells per mL (200 μL) per well and incubated for 24 h. The culture medium (100 μL) of the polymers-treated cells was collected and then treated with NO assay kit (Griess Reagent System, Promega Co., USA) according to the manufacturer's instructions. The absorbance was measured at 550 nm using a microplate reader. As a positive control, cells were treated with lipopolysaccharide (1 ng mL^{-1}) (LPS; FUJIFILM Wako Pure Chemical) for 24 h, and five independent tests were performed to evaluate NO production. The NO production was calculated by measuring the absorbance at 550 nm and comparing it with a calibration curve prepared using a standard solution of sodium nitrite.

Cell assay in injectable hydrogel

Mouse fibroblast NIH3T3 cells (ECACC, UK) were used for 3D cell culture experiments. The block copolymer (star-type $\mathbf{2_{118}}$) was sterilized by dry heat at 150 °C for 2 h prior to hydrogel preparation. The polymer was first dissolved in small amount of phosphate-buffered saline without calcium and magnesium ions (PBS (−)) at 4 °C for overnight, and then the media were added to the polymer solutions. The cells in DMEM containing 10% FBS and 1% penicillin/streptomycin (1.6×10^5 cells per mL (200 μL)) were added to the polymer solutions in a 96 well-plate and gently stirred by pipetting at 4 °C. With increasing the temperature to 37 °C, all polymers formed hydrogels even in cell-containing media. The resultant NIH3T3 cell-encapsulated hydrogels (15 wt%) were cultured at 37 °C under 5% CO_2 for 24 h. For the proliferation experiment, the NIH3T3 cell (1.6×10^3 cells per well)-encapsulated hydrogels were prepared in a 96 well-plate under serum media condition and cultured at 37 °C under 5% CO_2 for 1, 3 and 5 d. Then, the cells in the hydrogel (37 °C) were collected by centrifugation after cooling to 4 °C (sol state) to calculate the cell numbers. During these experiments, cell viability and the number of cells were evaluated using the WST-8 assay. For injectable experiments, a cell-containing polymer solution (4 °C) was loaded into a syringe (SS-01T, Terumo Co., Japan) and injected into a media at 37 °C to rapidly form hydrogel. The imaging of the live cells within the hydrogel was performed by confocal laser microscope (Nikon A1 confocal microscope, Nikon Solutions Co., Ltd, Japan) using a Cell Explorer™ (Cosmo Bio Co., Ltd, Japan).

Controlled release experiment

BSA and Dox were used as drug models for release experiment of the hydrogels. Fluorescent labelling of BSA was performed as previously described.[25] The drug model-loaded hydrogels (200 μL) were prepared by mixing the block copolymers (10 or 20 wt%) in PBS (−) with BSA–FITC (250 μM) or Dox (500 μM) at 4 °C and incubating the solution at 37 °C. The *in vitro* release experiments were carried out by immersing the above drug model-loaded hydrogels in a quartz cell filled with 2.8 mL of PBS (−) at 37 °C. The release profiles of BSA–FITC and Dox from the hydrogels were monitored using UV-vis spectroscopy. The concentrations of BSA–FITC and Dox were evaluated by measuring the absorbance at 499 and 480 nm, respectively. The cumulative drug release (BSA–FITC or Dox) was calculated from the amounts of drug-model loaded into the gel and released from the gel.

Results and discussion

Design and synthesis of amino acid-derived vinyl polymer/PEG hybrid block copolymers

Novel thermo-responsive amino acid-based block copolymers with linear and star-shaped structures were designed and

prepared by ATRP method. These copolymers comprised two distinct blocks: (i) an amino acid-derived vinyl polymer (LCST-type) acting as a thermo-switch for hydrophobic/hydrophilic character, and (ii) linear or 4-arm PEG (average MW: approximately 10 000), which enhances the total water-swollen structure. Previously, we constructed an amino acid-derived vinyl monomer library with a wide variety of hydropathy indices (*N*-acryloyl-X_{aa}-methyl ester, X_{aa} = Ala, β-Ala, Val, Leu, Phe, Gly, Ser, and Lys)[47] and conducted controlled radical polymerizations such as nitroxide-mediated radical polymerization (NMP),[44,48] ATRP,[42] and reversible addition fragmentation chain transfer (RAFT) polymerization.[45–47] Importantly, the transition temperatures (T_t) of the resultant LCST-type vinyl polymers systematically reflected the hydrophobicity of the constituent amino acids; that is, T_t shifted to a lower temperature with increasing polymer hydrophobicity. Here, relatively hydrophobic PNAAMe was employed because its T_t is approximately 18 °C[41] well below body temperature (~37 °C) (suitable for dynamic temperature change in biomedical field to trigger gelation *via* dehydration).

PEG is a well-known biocompatible polymer that is commonly used in cosmetics, pharmaceuticals, and biomedicine due to its good water solubility and nonfouling properties.[49,50] Tetra-PEG (4-arm) has also been reported as a useful building block for constructing ideal networks with homogeneity and low entanglement.[51] Thus, we anticipate that the 4-arm PEG block will facilitate network formation through dehydration of the PNAAMe block above T_t and suppress micelle/flower micelle formation, which is often observed in ABA-type triblock copolymers with hydrophobic–hydrophilic–hydrophobic patterns.[52–54]

First, two types of bromo-terminated PEG macroinitiators (linear and star-type) were prepared by the reaction of commercially available PEG or 4-arm PEG-NH_2 with 2-bromoisobutyryl bromide (Fig. S1 and S2, ESI†). The ATRPs of NAAMe using these PEG initiators were then conducted in methanol, and the resultant polymers were purified by reprecipitation using diethyl ether and dialysis against water. The chemical structures and molecular weights of the polymers were characterized by ^{1}H-NMR and SEC analyses. The SEC traces are unimodal with relatively narrow molecular weight distribution ($Đ$ = 1.13–1.29) (Fig. S5, ESI†), and shifted to higher molecular weight after ATRP. ^{1}H-NMR analyses also confirmed their chemical structures (Fig. S3 and S4, ESI†), indicating successful block polymerization. To elucidate the effects of the hydrophobic/hydrophilic block balance and polymer shape on hydrogel properties, six distinct block polymers with different PNAAMe lengths (n) (linear ($\mathbf{1}_n$) and star-type ($\mathbf{2}_n$)) were prepared by changing the monomer conversion and feed composition ([M]/[I]) (Table 1).

Hydrogel characteristics and thermo-responsiveness

All the PNAAMe/PEG block copolymers were soluble in water at low temperatures and exhibited LCST behavior. Fig. 2 illustrates the temperature dependence of the transmittance at 600 nm for typical block copolymers with the longest PNAAMe chains ($\mathbf{1}_{321}$ (weight fraction of PNAAMe units in the polymer: F_{PNAAMe} = 91 wt%) and $\mathbf{2}_{118}$ (F_{PNAAMe} = 88 wt%)) in pure water under dilute conditions (1 wt%) during the heating and cooling processes. Both linear and star-type polymers exhibited a phase separation with T_t of approximately 20 °C, which corresponds to the dehydration of PNAAMe blocks (T_t (PNAAMe homopolymer) = 18 °C), even when conjugated to PEG blocks. The LCST behaviors of $\mathbf{1}_{321}$ and $\mathbf{2}_{118}$ were reversible; namely, the turbid solution (above T_t) turns transparent upon cooling, although a slight hysteresis was observed in the heating and cooling curves owing to the delayed hydration of the polymer chains upon cooling. Interestingly, the transmittance of linear $\mathbf{1}_{321}$ aqueous solution above T_t was significantly higher than that of star $\mathbf{2}_{118}$ despite having almost the same F_{PNAAMe} values (hydrophobic/hydrophilic balance), and the transition curve displaying a gradual slope. This is probably due to the fact that the amphiphilic ABA-type triblock polymers with hydrophobic–hydrophilic–hydrophobic patterns tend to form micelles/flower micelles, which improves the dispersibility in water.[52–54] We previously reported that the triblock copolymer PNAAMe-*b*-poly(*N*-acryloyl glycine methyl ester)(PNAGMe)-*b*-PNAAMe forms a flower-like micellar structure with a dehydrated PNAAMe hydrophobic core and a looped PNAGMe hydrophilic shell.[54]

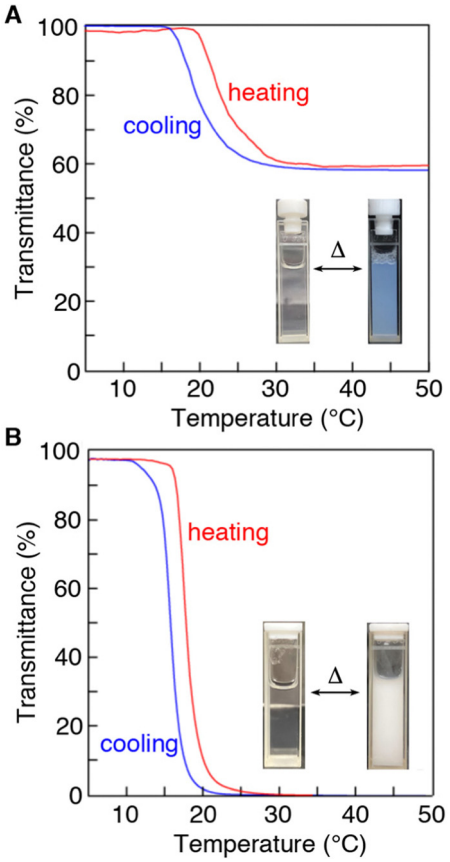

Fig. 2 Temperature dependences of transmittance at 600 nm for PNAAMe/PEG block copolymers with linear-type $\mathbf{1}_{321}$ (A) and star-shape $\mathbf{2}_{118}$ (B) in water (1 wt%) during heating (red line) and cooling (blue line) processes. Insets in (A) and (B) show photographs of the corresponding polymer solutions at 4 and 37 °C, respectively.

The gelation behaviors of $\mathbf{1}_n$ and $\mathbf{2}_n$ were subsequently investigated in concentrated aqueous solutions (>5 wt%) by the test tube inversion method. All polymer aqueous solutions were in the sol state at low temperature of 4 °C even at high concentration (25 wt%), while the polymers formed free-standing and milky hydrogels by heating to 37 °C, as depicted in the photographs of Fig. 3A and Fig. S6 (ESI†). A minimum polymer concentration was determined to be 6–25 wt% depending on the PNAAMe length and polymer shape, to form a hydrogel at 37 °C (Fig. 3B). Specifically, the minimum gelation concentration of $\mathbf{2}_n$ (6–13 wt%) was significantly lower than that of $\mathbf{1}_n$ (17–25 wt%), indicating the high gelation ability of the star-shaped polymers. Increasing the chain length of the PNAAMe blocks caused a systematic increase in gelation ability. Importantly, this sol-to-gel transition occurs rapidly and reversibly in response to temperature, including physiological temperature.

To gain further insight into gelation, rheological measurements were performed for $\mathbf{1}_{321}$ and $\mathbf{2}_{118}$ at the same concentration (25 wt%). The storage (G') and loss (G'') moduli are presented as functions of the temperature at 1% strain and 6.3 rad s^{-1} in Fig. 4(A and B). In both cases, in low temperature region below 20 °C, the G' value was considerably small and lower than G'' value ($G'' > G'$), demonstrating that polymer solutions were in a fluid sol state. With elevating temperature, the G' value increased drastically at around 22 °C (which is well consistent with T_t of PNAAMe block) and reversed with the G'' value ($G' > G''$). This phenomenon demonstrated that the dehydrated PNAAMe blocks, both in the linear and star polymers, formed crosslinking points in the hydrogel network through hydrophobic interactions. However, the hydrogel stiffness at 37 °C prepared from star-type was significantly higher (G' = 950 Pa) than that for linear-type (G' = 600 Pa) at same polymer concentration. Thus, the star-shape appears to be convenient for enhancing the crosslinking density. Note that the G' values of $\mathbf{1}_n$- and $\mathbf{2}_n$-hydrogels at 37 °C also depended on the chain length of the PNAAMe blocks when compared at the same concentration; namely, the stiffness was found to increase systematically corresponding the increase in the chain length (Fig. 4 and Fig. S7, ESI†). In this system, the hydrogel stiffness can be tuned by varying the polymer concentration, PNAAMe length, and polymer shape (Fig. S8, ESI†). Such mechanical tunability of hydrogels is important for biomedical applications such as mimicking various tissues and controlling retention at target sites *in vivo*.

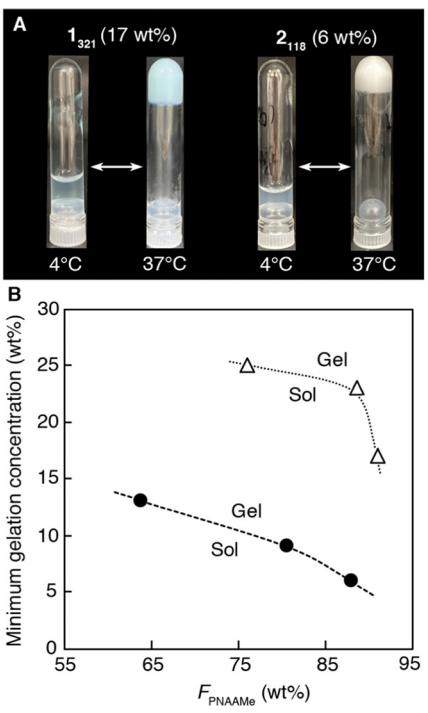

Fig. 3 (A) Photographs of thermo-reversible gelation of $\mathbf{1}_{321}$ (17 wt%) and $\mathbf{2}_{118}$ (6 wt%) block copolymers in pure water. (B) Plots of minimum gelation concentrations for $\mathbf{1}_n$ (open triangle) and $\mathbf{2}_n$ (closed circle) as a function of F_{PNAAMe} values.

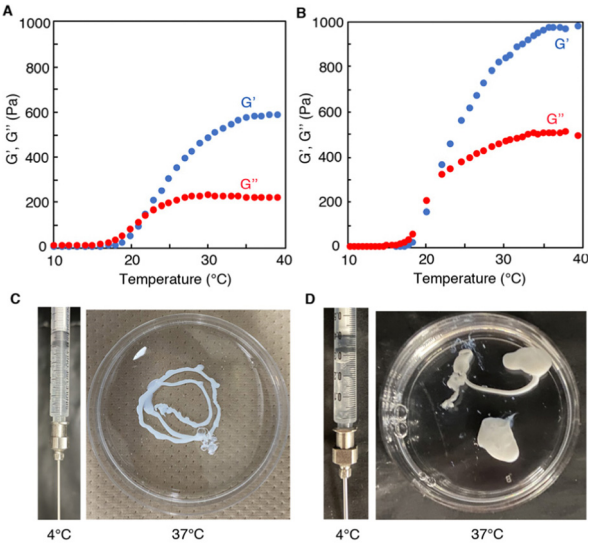

Fig. 4 Temperature dependences of the storage (G') and loss (G'') moduli for $\mathbf{1}_{321}$ (A) and $\mathbf{2}_{118}$ (B) from 10 to 40 °C at 6.3 rad s^{-1}, strain 1%. [polymer] = 25 wt%. (C and D) Photographs taken when the $\mathbf{1}_{321}$ (17 wt%) (C) and $\mathbf{2}_{118}$ (6 wt%) (D) aqueous solutions (4 °C) were injected into water (37 °C) by using a syringe, demonstrating the self-supporting hydrogel formation.

Subsequently, the injectability of these systems was explored based on their thermo-induced rapid gelation ability. Fig. 4(C and D) display photographs of the injection processes of $\mathbf{1}_{321}$ and $\mathbf{2}_{118}$. When the polymer solutions (4 °C) were extruded from a syringe into water at 37 °C (body temperature), hydrogelation occurred immediately due to the sharp LCST behavior of PNAAMe blocks. The resultant self-supporting hydrogels were stable in water at 37 °C whose injected shape had been maintained for at least one week. Evidently, these hydrogels can be re-dissolved promptly in water by re-cooling to 4 °C (below the T_t). Furthermore, the hydrogel possessed excellent shear-thinning and rapid self-healing capabilities owing to reversible physical cross-linkages *via* hydrophobic interactions (Fig. S9, ESI†). When large shear stress was applied to the $\mathbf{2}_{118}$-hydrogel, a decrease in the G' value was detected, and it transitioned to

the sol state. After release of the applied stress (the strain back to 1%), G' recovered quickly to almost 100% of the original state. Thus, these hydrogel systems can successfully exhibit injection capabilities *via* biological temperature-responsive and shear-thinning mechanisms.

In vitro assay of the injectable hydrogels as 3D-cell scaffold and controlled release materials

Since these injectable hydrogels can encapsulate various (bio)-molecules by simply mixing them when they are in a sol state below T_t (*ca.* 20 °C), we next investigated the ability of the hydrogels as an artificial ECM and a controlled release carrier. To assess the biocompatibility of the polymers, the cytotoxicity and stimulatory effects of $\mathbf{1}_n$ and $\mathbf{2}_n$ were evaluated *in vitro* using a mouse macrophage-like cell line (RAW264.7). PEG, a well-known biocompatible synthetic polymer, was used as a negative control for comparison. Fig. 5A shows the relative cell viabilities evaluated by WST-8 assay in the presence of $\mathbf{1}_{321}$ and $\mathbf{2}_{118}$ at concentrations ranging from 0.01 to 10 mg mL^{-1} for 24 h. The viability was approximately 90% in both cases, which was the same as that for PEG, even at high polymer concentrations (10 mg mL^{-1}). Similar results were observed for $\mathbf{1}_n$ and $\mathbf{2}_n$ with different PNAAMe chain lengths (Fig. S10(A and B), ESI†), demonstrating that both $\mathbf{1}_n$ and $\mathbf{2}_n$ were intrinsically non-toxic.

The stimulatory effects of $\mathbf{1}_n$ and $\mathbf{2}_n$ were evaluated using an NO assay. Macrophages, including RAW264.7, generate NO upon stimulation by stimulatory reagents such as liposaccharide (LPS).[55] Therefore, NO production *via* cells is a useful indicator for evaluating the stimulatory effects of polymers,[56] such as the activation of inflammatory signaling. Fig. 5B and Fig. S10(C and D) (ESI†) show the NO production tests for RAW264.7 cells treated with $\mathbf{1}_n$, $\mathbf{2}_n$, and LPS (1 ng mL^{-1}) (positive control) for 24 h. All polymers did not induce NO production in RAW264.7 cells even at high concentrations, demonstrating the negligible stimulatory and inflammatory effects of these polymers regardless of the differences in PNAAMe lengths and polymer shape. These results demonstrated that the PNAAMe/PEG block copolymers designed in this study possessed good biocompatibility for biological applications.

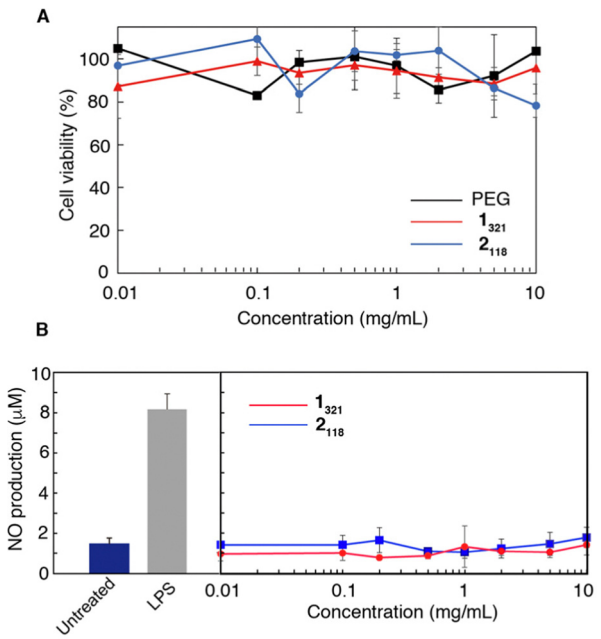

Fig. 5 Biocompatibility tests for the PNAAMe/PEG block copolymers, $\mathbf{1}_{321}$ and $\mathbf{2}_{118}$. (A) Cell viability (RAW264.7) cultured for 24 h in the presence of $\mathbf{1}_{321}$, $\mathbf{2}_{118}$, and PEG (0.01–10 mg mL^{-1}) using the WST-8 assay. Error bars represent the standard deviation (N = 3). (B) Summary of NO production from the RAW264.7 cells cultured for 24 h in the presence of the polymers. The same experiments were also carried out on TC-PSt, both with LPS (1 ng mL^{-1}) as a positive control and without LPS as a negative control. Error bars represent the standard deviation (N = 5).

Hence, we investigated the feasibility of using star-shaped $\mathbf{2}_{118}$-hydrogel as an injectable 3D ECM. Mouse fibroblast cell line (NIH3T3) was used for this study and encapsulated in $\mathbf{2}_{118}$-hydrogel by mixing the polymer aqueous solution (15 wt%, PBS (−)) at 4 °C and elevating the temperature to 37 °C. Then, the cell-encapsulated hydrogel was cultured at 37 °C in serum medium for 24 h. Importantly, the polymers could form hydrogel even in PBS (−) and serum medium in response to temperature manipulation. As shown in Fig. 6A, the live cells were found to be distributed homogeneously throughout the hydrogel after 24 h without any precipitation, reflecting the sufficient stiffness of the gel (G' = 650–950 Pa). In fact, the importance of gel stiffness as a cell scaffold had been previously discussed in supramolecular hydrogel systems constructed from amphiphilic peptides, where the lack of gel stiffness ($G' < 100$ Pa) leads to cell precipitation,[57] and a gel with 500 Pa stiffness shows *in vivo* retention at the target site without any dissolution into the surrounding tissue.[23] The cell viability in the $\mathbf{2}_{118}$-hydrogel, which was evaluated using the WST-8 assay, was close to 90% after 24 h (Fig. 6B). Notably, the hydrogel is injectable and can encapsulate live cells within the gel based on the rapid sol-to-gel transition simply by injecting the polymer/cell dispersion (4 °C) into the medium (37 °C) through a syringe (Fig. 6C). To further assess the ability of the hydrogels to act as 3D scaffolds, the proliferation behavior of the cells was studied in a hydrogel matrix under serum medium conditions (Fig. 6D). The same experiment was conducted using tissue culture polystyrene (TC-PSt) for comparison. Although the rate of cell proliferation in the hydrogel was slower than that on TC-PSt, NIH3T3 cells grew well in the hydrogel matrix. The hydrophobic crosslinking points present in the hydrogel, owing to the dehydration of the PNAAMe blocks, appear to function well as scaffolds for cell adhesion to the gel. In addition, cultured cells can be easily harvested using the gel-to-sol transition through temperature manipulation, which is an advantage of this hydrogel system.

Finally, we studied the controlled release of $\mathbf{2}_n$-hydrogels (20 wt%) *in vitro*. FITC-labeled BSA and Dox were selected as the protein drug model and anticancer agent, respectively. Fig. 7A depicts the cumulative amount of BSA-FITC released from $\mathbf{2}_n$-hydrogels in PBS (−) at 37 °C as a function of time. Sustained release was observed for all hydrogels. More importantly, the release profiles differed significantly depending on the chain length of the PNAAMe blocks even at the same total polymer

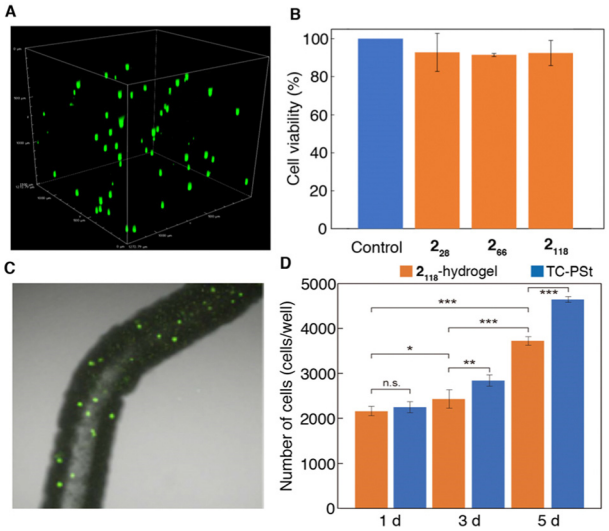

Fig. 6 (A) Confocal microscopy image of NIH3T3 cells in $\mathbf{2_{118}}$-hydrogel. The cells were cultured for 24 h in the hydrogel, and were stained with Cell Explorer™ Live Cell Tracking Kit. (B) Cell viability cultured for 24 h in $\mathbf{2_n}$-hydrogels (n = 28, 66, and 118) using the WST-8 assay. (C) Confocal microscopy image of NIH3T3 cells in $\mathbf{2_{118}}$-hydrogel obtained after being injected from a syringe and then cultured for 24 h. (D) Proliferation behaviors of the NIH/3T3 cells in the hydrogels (1.6×10^3 cells per well (96-well plate)). The number of the cells was calculated by WST-8 assay. Error bars represent the standard deviation (N = 5). *$p < 0.05$, **$p < 0.01$, ***$p < 0.001$, n.s.: not significant.

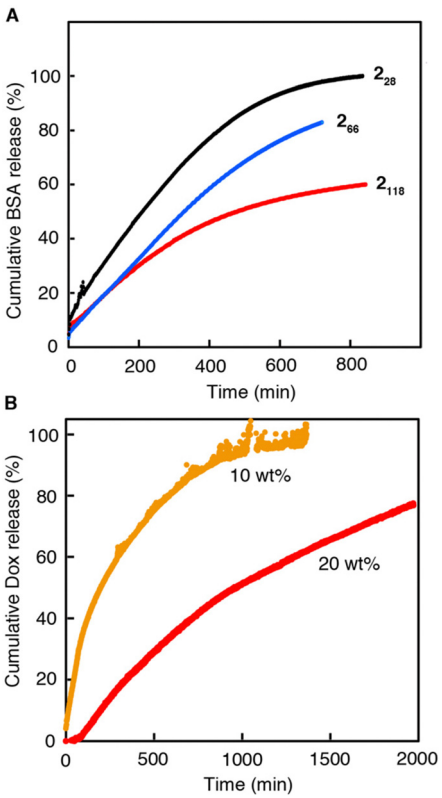

Fig. 7 Time dependences of cumulative amount of BSA–FITC released from the $\mathbf{2_n}$-hydrogels (n = 28, 66, and 118) (20 wt%) (A) and Dox from $\mathbf{2_{118}}$-hydrogels (10 and 20 wt%) (B) incubated in PBS (–) (pH 7.4) at 37 °C.

concentration. Increasing the length of PNAAMe caused a decelerated release of BSA–FITC from the gels. As described above, an increase in the PNAAMe length increases both the stiffness and network density, which likely enhances model protein drug retention. A similar controlled release of $\mathbf{2_{118}}$-hydrogel for Dox was also achieved, and its release behavior could be controlled by varying the polymer concentration during gel preparation (Fig. 7B). At 20 wt% hydrogel, approximately 70% of Dox was released from the gel after ~30 h. A much slower sustained release was previously observed for supramolecular peptide hydrogel systems, which released only ~30% Dox within 72–120 h, as a result of strong non-covalent interactions of Dox with peptide scaffolds, including electrostatic, π–π stacking, cation–π, and hydrophobic interactions.[58,59] Thus, the relatively fast release observed in our system indicated a weak interaction between Dox and the matrix. Therefore, the release profile of Dox can be tuned more precisely by partially introducing different amino acid units that can interact with Dox into the PNAAMe block through simple copolymerization.

Overall, the injectable and thermo-responsive 3D networks of these hydrogel systems composed of PNAAMe/PEG block copolymers, as well as their excellent biocompatibility, offer several exciting applications, such as a matrix for spatially and temporally controlled delivery/release of cells and therapeutics, and inks for 3D bioprinting.[60]

Conclusions

In conclusion, we have described the preparation of novel injectable hydrogels composed of thermo-responsive amino acid-derived vinyl polymers and PEGs with different polymer shapes, which were successfully synthesized *via* the ATRP of NAAMe using linear and star-shaped PEG macroinitiators. These block polymers are intrinsically nontoxic and exhibit LCST behavior below body temperature. At high concentrations, hydrogels were formed above T_t based on the dehydration of the PNAAMe blocks, which acted as thermo-reversible cross-linking points for the self-assembled polymer network. The chain lengths of the PNAAMe blocks (hydrophobic/hydrophilic balance) and the molecular shape (linear/star) affected the gel characteristics, including the gelation ability (that is, the minimum gel concentration) and rheological properties. Moreover, based on the highly rapid thermo-induced sol ($T < T_t$)-to-gel ($T > T_t$) transition and good biocompatibility of these gel systems, the hydrogels can act as injectable 3D-scaffolds for tissue engineering and sustained release applications. Notably, the thermo-responsiveness (for example, LCST/UCST, T_t, and microenvironment in the dehydrated state) of amino acid-derived vinyl polymers, as well as their chemical and physical properties, can be easily controlled by varying the type of amino acid units and their terminal structures. We believe that the smart hydrogel system presented in this study has great potential as a platform technology for designing various functional scaffolds for tissue engineering and sustained delivery of therapeutics tailored to specific biological applications.

Author contributions

T. K., S. N. and N. H. conceived the research and designed the experiments. M. N. and S. N. performed the experiments. T. K. and S. N. obtained funding for the project and oversaw the research. M. N. S. N., N. H., and T. K. co-wrote the manuscript. All authors discussed the results and commented on the manuscript.

Conflicts of interest

The authors declare no competing financial interests.

Acknowledgements

This work was supported by Grants-in-Aid for Scientific Research (KAKENHI) (JP22K05232 to T. K.) from the Japan Society for the Promotion of Science (JSPS). This research was also supported by Grant-in-Aid for the Japan Prize Foundation (to S. N.), Lotte Research Promotion Grant (to S. N.), and All Doshisha Research Model "SDGs Research Project" (to T. K. and S. N.).

Notes and references

1 O. Wichterle and D. Lím, *Nature*, 1960, **185**, 117–118.
2 D. Seliktar, *Science*, 2012, **336**, 1124–1128.
3 N. M. Sangeetha and U. Maitra, *Chem. Soc. Rev.*, 2005, **34**, 821–836.
4 A. S. Hoffman, *Adv. Drug Delivery Rev.*, 2013, **65**, 10–16.
5 Y. Okumura and K. Ito, *Adv. Mater.*, 2001, **13**, 485–487.
6 J. P. Gong, Y. Katsuyama, T. Kurokawa and Y. Osada, *Adv. Mater.*, 2003, **15**, 1155–1158.
7 J.-Y. Sun, X. Zhao, W. R. K. Illeperuma, O. Chaudhuri, K. H. Oh, D. J. Mooney, J. J. Vlassak and Z. Suo, *Nature*, 2012, **489**, 133–136.
8 M. Nakahata, Y. Takashima, H. Yamaguchi and A. Harada, *Nat. Commun.*, 2011, **2**, 511.
9 Y. Sun, A. L. Wollenberg, T. M. O'Shea, Y. Cui, Z. H. Zhou, M. V. Sofroniew and T. J. Deming, *J. Am. Chem. Soc.*, 2017, **139**, 15114–15121.
10 S. Talebian, M. Mehrali, N. Taebnia, C. P. Pennisi, F. B. Kadumudi, J. Foroughi, M. Hasany, M. Nikkhah, M. Akbari, G. Orive and A. Dolatshahi-Pirouz, *Adv. Sci.*, 2019, **6**, 1801664.
11 H. Rammal, A. GhavamiNejad, A. Erdem, R. Mbeleck, M. Nematollahi, S. Emir Diltemiz, H. Alem, M. A. Darabi, Y. N. Ertas, E. J. Caterson and N. Ashammakhi, *Mater. Chem. Front.*, 2021, **5**, 4368–4400.
12 C. Löwenberg, M. Balk, C. Wischke, M. Behl and A. Lendlein, *Acc. Chem. Res.*, 2017, **50**, 723–732.
13 J. Shang, X. Le, J. Zhang, T. Chen and P. Theato, *Polym. Chem.*, 2019, **10**, 1036–1055.
14 T. Koga, K. Tomimori and N. Higashi, *Macromol. Rapid Commun.*, 2020, **41**, 1900650.
15 K. Liang, K. H. Bae and M. Kurisawa, *J. Mater. Chem. B*, 2019, **7**, 3775–3791.
16 Y. Chao, Q. Chen and Z. Liu, *Adv. Funct. Mater.*, 2020, **30**, 1902785.
17 P. Bertsch, M. Diba, D. J. Mooney and S. C. G. Leeuwenburgh, *Chem. Rev.*, 2023, **123**, 834–873.
18 B. A. Aguado, W. Mulyasasmita, J. Su, K. J. Lampe and S. C. Heilshorn, *Tissue Eng., Part A*, 2012, **18**, 806–815.
19 C. Yan, M. E. Mackay, K. Czymmek, R. P. Nagarkar, J. P. Schneider and D. J. Pochan, *Langmuir*, 2012, **28**, 6076–6087.
20 J. S. Temenoff, H. Shin, D. E. Conway, P. S. Engel and A. G. Mikos, *Biomacromolecules*, 2003, **4**, 1605–1613.
21 X. Z. Shu, Y. Liu, F. S. Palumbo, Y. Luo and G. D. Prestwich, *Biomaterials*, 2004, **25**, 1339–1348.
22 B. D. Olsen, J. A. Kornfield and D. A. Tirrell, *Macromolecules*, 2010, **43**, 9094–9099.
23 E. L. Bakota, Y. Wang, F. R. Danesh and J. D. Hartgerink, *Biomacromolecules*, 2011, **12**, 1651–1657.
24 M. Guvendiren, H. D. Lu and J. A. Burdick, *Soft Matter*, 2012, **8**, 260–272.
25 T. Koga, T. Matsuoka, Y. Morita and N. Higashi, *Mater. Adv.*, 2021, **2**, 4068–4074.
26 B. Jeong, S. W. Kim and Y. H. Bae, *Adv. Drug Delivery Rev.*, 2012, **64**, 154–162.
27 L. Klouda and A. G. Mikos, *Eur. J. Pharm. Biopharm.*, 2008, **68**, 34–45.
28 M.-T. Popescu, G. Liontos, A. Avgeropoulos, E. Voulgari, K. Avgoustakis and C. Tsitsilianis, *ACS Appl. Mater. Interfaces*, 2016, **8**, 17539–17548.
29 A. Chenite, C. Chaput, D. Wang, C. Combes, M. D. Buschmann, C. D. Hoemann, J. C. Leroux, B. L. Atkinson, F. Binette and A. Selmani, *Biomaterials*, 2000, **21**, 2155–2161.
30 H. F. Darge, A. T. Andrgie, H.-C. Tsai and J.-Y. Lai, *Int. J. Biol. Macromol.*, 2019, **133**, 545–563.
31 S. H. Lee, Y. Lee, Y. W. Chun, S. W. Crowder, P. P. Young, K. D. Park and H.-J. Sung, *Adv. Funct. Mater.*, 2014, **24**, 6771–6781.
32 Z. Ren, Y. Wang, S. Ma, S. Duan, X. Yang, P. Gao, X. Zhang and Q. Cai, *ACS Appl. Mater. Interfaces*, 2015, **7**, 19006–19015.
33 X. Xu, Y. Liu, W. Fu, M. Yao, Z. Ding, J. Xuan, D. Li, S. Wang, Y. Xia and M. Cao, *Polymers*, 2020, **12**, 580.
34 B. Jeong, Y. H. Bae, D. S. Lee and S. W. Kim, *Nature*, 1997, **388**, 860–862.
35 A. Alexander, J. Khan, S. Saraf and S. Saraf, *J. Controlled Release*, 2013, **172**, 715–729.
36 K. Uchida, K. Sakai, E. Ito, O. H. Kwon, A. Kikuchi, M. Yamato and T. Okano, *Biomaterials*, 2000, **21**, 923–929.
37 Y. Zhang, J. Cai, C. Li, J. Wei, Z. Liu and W. Xue, *J. Mater. Chem. B*, 2016, **4**, 3733–3749.
38 H. Mori, H. Iwaya, A. Nagai and T. Endo, *Chem. Commun.*, 2005, 4872–4874.
39 J. Seuring, F. M. Bayer, K. Huber and S. Agarwal, *Macromolecules*, 2012, **45**, 374–384.
40 Y. Zhu, A. B. Lowe and P. J. Roth, *Polymer*, 2014, **55**, 4425–4431.
41 N. Higashi, R. Sonoda and T. Koga, *RSC Adv.*, 2015, **5**, 67652–67657.

42 N. Higashi, A. Hirata, S. Nishimura and T. Koga, *Colloids Surf., B*, 2017, **159**, 39–46.
43 K. Bauri, M. Nandi and P. De, *Polym. Chem.*, 2018, **9**, 1257–1287.
44 S. Nishimura, N. Higashi and T. Koga, *Chem. Commun.*, 2019, **55**, 1498–1501.
45 T. Yamano, N. Higashi and T. Koga, *Macromol. Rapid Commun.*, 2020, **41**, 1900550.
46 T. Yamano, N. Higashi and T. Koga, *Langmuir*, 2020, **36**, 6550–6556.
47 A. Sawamoto, S. Nishimura, N. Higashi and T. Koga, *Polym. Chem.*, 2023, **14**, 2857–2864.
48 S. Nishimura, N. Higashi and T. Koga, *Polym. Chem.*, 2019, **10**, 71–76.
49 J. M. Harris and R. B. Chess, *Nat. Rev. Drug Discovery*, 2003, **2**, 214–221.
50 C.-C. Lin and K. S. Anseth, *Pharm. Res.*, 2009, **26**, 631–643.
51 T. Sakai, Y. Akagi, T. Matsunaga, M. Kurakazu, U.-I. Chung and M. Shibayama, *Macromol. Rapid Commun.*, 2010, **31**, 1954–1959.
52 S. Honda, T. Yamamoto and Y. Tezuka, *J. Am. Chem. Soc.*, 2010, **132**, 10251–10253.
53 Y. Mizoue, E. Onodera, K. Haraguchi and S. Yusa, *Polymers*, 2022, **14**, 1678.
54 N. Higashi, S. Matsubara, S. Nishimura and T. Koga, *Materials*, 2018, **11**, 424.
55 C. Bogdan, *Nat. Immunol.*, 2001, **2**, 907–916.
56 S. Nishimura, K. Nishida, T. Ueda, S. Shiomoto and M. Tanaka, *Polym. Chem.*, 2022, **13**, 2519–2530.
57 C. Chen, Y. Gu, L. Deng, S. Han, X. Sun, Y. Chen, J. R. Lu and H. Xu, *ACS Appl. Mater. Interfaces*, 2014, **6**, 14360–14368.
58 S. Zarzhitsky and H. Rapaport, *J. Colloid Interface Sci.*, 2011, **360**, 525–531.
59 M. A. Elsawy, J. K. Wychowaniec, L. A. Castillo Díaz, A. M. Smith, A. F. Miller and A. Saiani, *Biomacromolecules*, 2022, **23**, 2624–2634.
60 D. M. Kirchmajer, R. Gorkin III and M. in het Panhuis, *J. Mater. Chem. B*, 2015, **3**, 4105–4117.